A Model of the Peritoneal Cavity for Use in Internal Dosimetry

E. E. Watson, M. G. Stabin, J. L. Davis*, and K. F. Eckerman

Oak Ridge Associated Universities, and Oak Ridge National Laboratory, Oak Ridge, Tennessee

Several therapeutic and diagnostic techniques involve injection of radioactive material into the peritoneal cavity. Estimation of the radiation dose to the surface of the pertioneum or to surrounding organs is hampered by the lack of a suitable source region in the phantom commonly used for such calculations. We have modified the Fisher-Snyder phantom to include a region representing the peritoneal cavity which may be employed to estimate such radiation doses. A geometric model is described which is coordinated with the existing organ regions in the phantom. Specific absorbed fractions (derived by Monte Carlo techniques) for photon emissions originating within the cavity are listed. Photon S-values for several radionuclides which have been administered intraperitoneally are shown. Dose conversion factors for electrons irradiating the peritoneal cavity wall, from either a thin plane or volume source of activity within the cavity, are also given for several nuclides.

J Nucl Med 30:2002–2011, 1989

For many years, one method used for controlling the recurrent effusions that result from malignant disease has been the intraperitoneal injection of radioactive materials (*1–3*). More recently, technetium-99m-(^{99m}Tc) labeled materials such as microspheres have been injected intraperitoneally to evaluate the patency of LeVeen peritoneovenous shunts (PVS) and to determine the distribution of radioactive materials used for therapy (*4–10*). Radionuclide hysterosalpingography also may result in some activity reaching the peritoneal cavity (*11*).

When radionuclides are injected or infused into a cavity, the material may be distributed over the walls of the cavity or in a volume of fluid within the cavity. This requires that dose components from the emissions usually classed as nonpenetrating (electrons, betas, etc.) be calculated at various distances from the source material. The doses from the photons also present special problems because the peritoneal cavity surrounds, but does not include, a number of abdominal organs. Because the Fisher-Snyder phantom (*12*) does not contain a source region which is an appropriate representation of this body space, attempts to calculate the radiation dose must be based on existing source regions which will not model the activity distribution very accurately (e.g., small intestine).

We have developed a mathematic model of the peritoneal cavity that permits standard Monte Carlo techniques to be used to derive specific absorbed fractions for photons to the major target organs of a modified version of the Fisher-Snyder phantom (*13*), which includes improved models for some organs and several organ regions not considered in the Fisher-Snyder phantom. We have used these specific absorbed fractions to calculate S-values for some radionuclides that have been administered intraperitoneally. In addition, we have calculated the doses in soft tissue near the cavity from betas and monoenergetic electrons emitted by these radionuclides. These values may represent absorbed dose in the peritoneal cavity wall or in portions of nearby organs or tissues.

METHODS

Peritoneal Cavity Model

The peritoneal cavity is a space defined by the mesothelial lining with surrounds various organs in the abdominal cavity (*14*). This lining, called the peritoneum, defines a kind of sac which lines the body cavity from the diaphragm to the pelvic floor. In males, it is a closed sac; in females, the sac communicates with the fallopian tubes. It consists of two parts, the general peritoneal cavity and the omental bursa, which are

Received Jan. 26, 1989; revision accepted Aug. 9, 1989.

For reprints contact: Evelyn E. Watson, Radiopharmaceutical Internal Dose Information Center, Oak Ridge Associated Universities, P.O. Box 117, Oak Ridge, TN 37831.

* Deceased.

TABLE 1
Specific Absorbed Fractions of Energy (g^{-1}) Source in Peritoneal Cavity Volume

Target organ	Energy (MeV) 0.010	0.015	0.020	0.030	0.050	0.100
Adrenals	0	0	9.5×10^{-6}	2.9×10^{-5}	3.9×10^{-5}	3.2×10^{-5}
Brain	0	0	0	0	2.5×10^{-9}	1.2×10^{-8}
Breasts	0	0	3.1×10^{-9}	2.7×10^{-7}	1.1×10^{-6}	1.8×10^{-6}
GI tract:						
LLI wall	0	0	2.7×10^{-7}	5.0×10^{-6}	1.1×10^{-5}	8.8×10^{-6}
Small int.	7.9×10^{-6}	2.5×10^{-5}	4.4×10^{-5}	5.8×10^{-5}	5.0×10^{-5}	3.5×10^{-5}
Stomach wall	0	0	2.0×10^{-6}	1.8×10^{-5}	2.8×10^{-5}	2.2×10^{-5}
ULI wall	5.1×10^{-7}	9.7×10^{-6}	2.8×10^{-5}	5.0×10^{-5}	4.4×10^{-5}	3.2×10^{-5}
Heart wall	0	7.4×10^{-7}	6.0×10^{-6}	1.8×10^{-5}	1.8×10^{-5}	1.3×10^{-5}
Kidneys	0	0	1.7×10^{-6}	1.7×10^{-5}	2.8×10^{-5}	2.3×10^{-5}
Liver	3.2×10^{-6}	9.2×10^{-6}	1.6×10^{-5}	2.4×10^{-5}	2.5×10^{-5}	2.0×10^{-5}
Lungs	0	8.7×10^{-9}	8.7×10^{-7}	4.3×10^{-6}	6.7×10^{-6}	5.4×10^{-6}
Ovaries	0	0	1.2×10^{-5}	3.2×10^{-5}	2.8×10^{-5}	2.0×10^{-5}
Pancreas	7.2×10^{-5}	1.7×10^{-4}	2.2×10^{-4}	1.9×10^{-4}	1.3×10^{-4}	7.9×10^{-5}
Muscle	1.9×10^{-5}	1.8×10^{-5}	1.6×10^{-5}	1.4×10^{-5}	9.9×10^{-6}	7.3×10^{-6}
Skeleton	0	6.0×10^{-8}	9.5×10^{-7}	5.6×10^{-6}	1.0×10^{-5}	6.9×10^{-6}
Bone surfaces	0	8.2×10^{-8}	1.4×10^{-6}	8.6×10^{-6}	1.7×10^{-5}	1.1×10^{-5}
Red marrow	0	4.4×10^{-8}	7.0×10^{-7}	4.1×10^{-6}	8.8×10^{-6}	9.4×10^{-6}
Skin	0	0	7.0×10^{-9}	3.1×10^{-7}	1.1×10^{-6}	1.4×10^{-6}
Spleen	0	0	1.9×10^{-7}	5.3×10^{-6}	1.2×10^{-5}	1.3×10^{-5}
Testes	0	0	0	0	7.8×10^{-7}	1.5×10^{-6}
Thymus	0	0	0	1.4×10^{-7}	2.3×10^{-6}	1.8×10^{-6}
Thyroid	0	0	0	0	1.7×10^{-7}	5.8×10^{-8}
Urinary bladder wall	0	1.8×10^{-7}	9.4×10^{-6}	1.9×10^{-5}	1.8×10^{-5}	1.4×10^{-5}
Uterus	1.1×10^{-4}	3.2×10^{-4}	4.1×10^{-4}	3.1×10^{-4}	1.5×10^{-4}	8.7×10^{-5}
Total body	1.4×10^{-5}	1.4×10^{-5}	1.4×10^{-5}	1.3×10^{-5}	1.1×10^{-5}	8.1×10^{-6}

	Energy (MeV) 0.200	0.500	1.000	1.500	2.000	4.000
Adrenals	2.6×10^{-5}	2.4×10^{-5}	2.2×10^{-5}	1.6×10^{-5}	1.3×10^{-5}	1.7×10^{-5}
Brain	1.7×10^{-8}	2.0×10^{-8}	1.0×10^{-7}	1.1×10^{-7}	1.3×10^{-7}	1.9×10^{-7}
Breasts	1.9×10^{-6}	1.8×10^{-6}	1.8×10^{-6}	2.3×10^{-6}	2.1×10^{-6}	1.9×10^{-6}
GI tract:						
LLI wall	8.0×10^{-6}	7.0×10^{-6}	6.0×10^{-6}	6.4×10^{-6}	6.4×10^{-6}	4.6×10^{-6}
Small int.	3.2×10^{-5}	2.9×10^{-5}	2.6×10^{-5}	2.4×10^{-5}	2.3×10^{-5}	1.8×10^{-5}
Stomach wall	1.9×10^{-5}	1.8×10^{-5}	1.6×10^{-5}	1.6×10^{-5}	1.4×10^{-5}	1.2×10^{-5}
ULI wall	2.7×10^{-5}	2.5×10^{-5}	2.3×10^{-5}	2.0×10^{-5}	2.1×10^{-5}	1.6×10^{-5}
Heart wall	1.2×10^{-5}	1.1×10^{-5}	1.1×10^{-5}	9.6×10^{-6}	9.6×10^{-6}	7.5×10^{-6}
Kidneys	2.1×10^{-5}	1.9×10^{-5}	1.8×10^{-5}	1.6×10^{-5}	1.6×10^{-5}	1.2×10^{-5}
Liver	1.7×10^{-5}	1.6×10^{-5}	1.5×10^{-5}	1.4×10^{-5}	1.3×10^{-5}	1.1×10^{-5}
Lungs	5.0×10^{-6}	5.0×10^{-6}	4.5×10^{-6}	4.3×10^{-6}	4.1×10^{-6}	3.3×10^{-6}
Ovaries	2.0×10^{-5}	2.1×10^{-5}	1.8×10^{-5}	1.8×10^{-5}	1.6×10^{-5}	1.5×10^{-5}
Pancreas	7.3×10^{-5}	7.1×10^{-5}	6.0×10^{-5}	5.8×10^{-5}	5.2×10^{-5}	4.1×10^{-5}
Muscle	6.8×10^{-6}	6.7×10^{-6}	6.3×10^{-6}	5.9×10^{-6}	5.5×10^{-6}	4.5×10^{-6}
Skeleton	4.4×10^{-6}	3.3×10^{-6}	2.9×10^{-6}	2.9×10^{-6}	2.7×10^{-6}	2.3×10^{-6}
Bone surf.	6.1×10^{-6}	4.1×10^{-6}	3.5×10^{-6}	3.4×10^{-6}	3.2×10^{-6}	2.7×10^{-6}
Red marrow	8.9×10^{-6}	8.4×10^{-6}	7.9×10^{-6}	7.6×10^{-6}	7.2×10^{-6}	5.9×10^{-6}
Skin	1.5×10^{-6}	1.7×10^{-6}	1.8×10^{-6}	1.6×10^{-6}	1.6×10^{-6}	1.4×10^{-6}
Spleen	1.1×10^{-5}	1.0×10^{-5}	9.2×10^{-6}	8.7×10^{-6}	7.7×10^{-6}	7.0×10^{-6}
Testes	1.3×10^{-6}	1.1×10^{-6}	1.1×10^{-6}	1.2×10^{-6}	1.5×10^{-6}	9.0×10^{-7}
Thymus	1.7×10^{-6}	2.0×10^{-6}	2.5×10^{-6}	6.2×10^{-7}	1.6×10^{-6}	2.5×10^{-6}
Thyroid	2.4×10^{-8}	4.4×10^{-7}	6.2×10^{-7}	4.8×10^{-7}	4.5×10^{-7}	5.5×10^{-7}
Urinary bladder wall	1.1×10^{-5}	1.4×10^{-5}	9.8×10^{-6}	9.7×10^{-6}	9.2×10^{-6}	9.2×10^{-6}
Uterus	8.0×10^{-5}	8.6×10^{-5}	7.2×10^{-5}	7.0×10^{-5}	6.5×10^{-5}	4.8×10^{-5}
Total body	7.2×10^{-6}	6.9×10^{-6}	6.4×10^{-6}	6.0×10^{-6}	5.6×10^{-6}	4.6×10^{-6}

TABLE 2
Photon S-Values for Technetium-99m in Peritoneal Cavity Volume

Target organ	S-Value (mGy/MBq-sec)	S-Value (rad/μCi-hr)
Red marrow	1.8×10^{-7}	2.4×10^{-6}
Bone surfaces	1.8×10^{-7}	2.4×10^{-6}
Adrenals	5.9×10^{-7}	7.8×10^{-6}
Brain	2.8×10^{-10}	3.7×10^{-9}
Breasts	3.7×10^{-8}	4.9×10^{-7}
Lower large intestine wall	1.7×10^{-7}	2.2×10^{-6}
Small intestine	6.8×10^{-7}	9.1×10^{-6}
Stomach wall	4.2×10^{-7}	5.5×10^{-6}
Upper large intestine wall	6.0×10^{-7}	8.0×10^{-6}
Heart wall	2.6×10^{-7}	3.4×10^{-6}
Kidneys	4.4×10^{-7}	5.9×10^{-6}
Liver	3.7×10^{-7}	5.0×10^{-6}
Lungs	1.0×10^{-7}	1.4×10^{-6}
Ovaries	4.0×10^{-7}	5.4×10^{-6}
Pancreas	1.6×10^{-6}	2.1×10^{-5}
Remaining tissue (muscle)	1.5×10^{-7}	1.9×10^{-6}
Skeleton	1.2×10^{-7}	1.6×10^{-6}
Skin	2.8×10^{-7}	3.7×10^{-6}
Spleen	2.4×10^{-7}	3.2×10^{-6}
Testes	2.8×10^{-8}	3.7×10^{-7}
Thymus	3.5×10^{-8}	4.6×10^{-7}
Thyroid	8.9×10^{-10}	1.2×10^{-8}
Urinary bladder wall	2.6×10^{-7}	3.5×10^{-6}
Uterus	1.8×10^{-6}	2.4×10^{-5}
Total body	1.6×10^{-7}	2.1×10^{-6}

connected. The cavity lining has a highly variable thickness. Measured values in adults range from 0.5 to 2 mm, with an average of 1–1.5 mm (personal communication: Carol Marcus, MD, Harbor UCLA Medical Center). These values are highly variable both among individuals and in different locations within an individual, and are subject to further variability caused by stretching.

The cavity is structurally complex and is extremely difficult to model accurately because of its many complex folds and invaginations. All organs are actually outside of the cavity; however, organs which have a major portion of their surfaces covered by the visceral peritoneum appear to be inside the cavity. Normally, the cavity contains a very slight amount of watery fluid which tends to lubricate its inner surfaces. In pathologic conditions, however, the cavity may become greatly distended with fluid.

For dosimetry purposes, organs surrounded by the cavity may be modeled as being within a large cylinder whose boundaries correspond to the outer boundaries of the peritoneum. For Monte Carlo simulation of photon transport, acceptable results will be obtained if the geometry of the source region is a reasonable representation of the actual organ or system. We chose to model the cavity as two connected elliptical cylinders. The upper cylinder has a section removed on the posterior side to account for the fact that the cavity does not surround the spine, adrenals, or kidneys. This cylinder runs along the inner surface of the ribs, thus surrounding the liver and all other major organs in the abdomen above the pelvis to the top of the liver. The lower cylinder is only slightly larger than the small intestine, and extends downward to the top of the urinary bladder. This cylinder is restricted to cause its outer surface to conform in shape to that of the small intestine. The following equations describe this mathematically. The x, y, and z conventions in the Fisher-Snyder phantom (*12*) are used, namely that x is positive to the phantom's left, y is positive to the rear of the phantom and z is positive upward, with the origin at the juncture of the trunk and the legs in the center of the trunk ellipse.

$$11.5 \le z \le 27: \left(\frac{x}{11.3}\right)^2 + \left(\frac{y}{11.3}\right)^2 \le 1 \qquad -7 \le y \le 3$$

$$27 \le z \le 38: \left(\frac{x}{16.5}\right)^2 + \left(\frac{y}{9.3}\right)^2 \le 1$$

$$y < -3.0 * \left[1 - \left(\frac{x}{A}\right)^2\right]^{1/2} + 5.5 \qquad -A \le x \le A$$

$$A = 4.5 * \left[1 - \left(\frac{z - 32.5}{5.5}\right)^2\right]^{1/2} + 6.0$$

$$38 \le z \le 43: \left(\frac{x}{16.5}\right)^2 + \left(\frac{y}{9.3}\right)^2 \le 1$$

$$y < -2.5 * \left[1 - \left(\frac{x}{4.5}\right)^2\right]^{1/2} + 5.5 \qquad -4.5 \le x \le 4.5$$

The variable diameter between z = 27 and z = 38 allows the kidneys to fit outside of the cavity. Figure 1 shows some computer-generated drawings of cross sections of the body which illustrate the placement of the peritoneal cavity bound-

TABLE 3
Photon S-Values for Indium-111 in Peritoneal Cavity Volume

Target organ	S-Value (mGy/MBq-sec)	S-Value (rad/μCi-hr)
Red marrow	5.5×10^{-7}	7.4×10^{-6}
Bone surfaces	4.1×10^{-7}	5.5×10^{-6}
Adrenals	1.7×10^{-6}	2.2×10^{-5}
Brain	1.0×10^{-9}	1.4×10^{-8}
Breasts	1.2×10^{-7}	1.5×10^{-6}
Lower large intestine wall	5.0×10^{-7}	6.7×10^{-6}
Small intestine	1.8×10^{-6}	2.4×10^{-5}
Stomach	7.7×10^{-7}	1.0×10^{-5}
Upper large intestine wall	1.8×10^{-6}	2.4×10^{-5}
Heart wall	7.7×10^{-7}	1.0×10^{-5}
Kidneys	1.3×10^{-6}	1.8×10^{-5}
Liver	1.1×10^{-6}	1.5×10^{-5}
Lungs	3.2×10^{-7}	4.2×10^{-6}
Ovaries	1.3×10^{-6}	1.8×10^{-5}
Pancreas	5.2×10^{-6}	6.9×10^{-5}
Remaining tissue (muscle)	4.7×10^{-7}	6.3×10^{-6}
Skeleton	2.9×10^{-7}	3.9×10^{-6}
Skin	9.1×10^{-8}	1.2×10^{-6}
Spleen	7.0×10^{-7}	9.4×10^{-6}
Testes	7.8×10^{-8}	1.0×10^{-6}
Thymus	1.1×10^{-7}	1.4×10^{-6}
Thyroid	4.0×10^{-9}	5.3×10^{-8}
Urinary bladder wall	7.6×10^{-7}	1.0×10^{-5}
Uterus	6.2×10^{-6}	8.3×10^{-5}
Total body	4.9×10^{-7}	6.6×10^{-6}

TABLE 4
Photon S-Values for Iodine-125 in Peritoneal Cavity Volume

Target organ	S-Value (mGy/MBq-sec)	S-Value (rad/μCi-hr)
Red marrow	4.2×10^{-8}	5.6×10^{-7}
Bone surfaces	4.6×10^{-8}	6.1×10^{-7}
Adrenals	1.8×10^{-7}	2.4×10^{-6}
Brain	5.8×10^{-11}	7.8×10^{-10}
Breasts	7.0×10^{-9}	9.4×10^{-8}
Lower large intestine wall	4.1×10^{-8}	5.4×10^{-7}
Small intestine	2.9×10^{-7}	3.8×10^{-6}
Stomach	1.2×10^{-7}	1.5×10^{-6}
Upper large intestine wall	2.4×10^{-7}	3.2×10^{-6}
Heart wall	9.2×10^{-8}	1.2×10^{-6}
Kidneys	1.2×10^{-7}	1.6×10^{-6}
Liver	1.3×10^{-7}	1.7×10^{-6}
Lungs	3.0×10^{-8}	3.9×10^{-7}
Ovaries	1.6×10^{-7}	2.2×10^{-6}
Pancreas	8.9×10^{-7}	1.2×10^{-5}
Remaining tissue (muscle)	6.9×10^{-8}	9.2×10^{-7}
Skeleton	3.1×10^{-8}	4.1×10^{-7}
Skin	6.0×10^{-9}	8.0×10^{-8}
Spleen	5.2×10^{-8}	7.0×10^{-7}
Testes	4.1×10^{-9}	5.5×10^{-8}
Thymus	6.6×10^{-9}	8.7×10^{-8}
Thyroid	4.4×10^{-10}	5.9×10^{-9}
Urinary bladder wall	9.7×10^{-8}	1.3×10^{-6}
Uterus	1.3×10^{-6}	1.8×10^{-5}
Total body	6.8×10^{-8}	9.1×10^{-7}

aries. For comparison, see figures XI-37 and XI-38 from Morris' Human Anatomy (*14*) which illustrate some of the relationships between the peritoneal cavity and the abdominal organs.

In this model, the cavity encloses the liver, spleen, gallbladder, ovaries, uterus, stomach, pancreas, small intestine, and upper and lower large intestine while excluding the kidneys, adrenals, urinary bladder, and all bone structures. The volume of the model is certainly larger than the volume of the cavity because it includes many spaces in the body which are actually filled with soft tissue. For purposes of simulating photon transport, however, the geometry is representative of the cavity structure. Calculating the volume of the model is difficult because of the irregular geometry in the upper cylinder, but numerical techniques using Gauss quadrature integration techniques (*15*) yield a satisfactory answer. In the lower cylinder, the volume was calculated analytically, but corrections were made for volumes of abdominal organs included in the cavity which are within the small intestine boundaries or which continue outside of the peritoneal cavity boundaries. The approximate volume of the cavity in the model is 5650 cm^3. The largest value found in the literature for cavity volume is 4000 cm^3 (*16*). This approximation is adequate for Monte Carlo simulation of photon transport, for the reasons stated above.

Knowledge of the exact wall thickness is not critical to the calculations. The wall is too thin to represent a scoring region in the Monte Carlo analysis because too few photon "hits" would occur to permit the extraction of statistically valid results. As will be seen in the dose calculations, the dose to the wall is dominated by the nonpenetrating emission contributions.

Calculation of Photon S-Values

The mathematic model of the peritoneal cavity was used to generate specific absorbed fractions for 0.010, 0.015, 0.020, 0.030, 0.050, 0.100, 0.200, 0.500, 1.0, 1.5, 2.0, and 4.0 MeV photons. Random positions within the cavity for generation of a photon were chosen by randomly sampling within the entire cavity and rejecting any points which fell within defined organ regions of the phantom. All of the major abdominal organs plus the active marrow, bone surfaces, brain, and breasts were included as target organs. Photon S-values were calculated for gold-198 (^{198}Au), iodine-125 (^{125}I), iodine-131 (^{131}I), and ^{99m}Tc.

Phosphorus-32 and yttrium-90 (^{90}Y) do not emit photons in their decay schemes and, therefore, do not irradiate the abdominal organs to the same extent as ^{198}Au, ^{131}I, and ^{99m}Tc. Some contribution from bremsstrahlung radiation will result, as shown by Williams et al. (*17*) and Stabin et al. (*18*). This contribution was not treated in this work, but may be estimated by folding the bremsstrahlung spectrum for these nuclides over the specific absorbed fractions given in Table 1.

Calculation of Dose to the Peritoneal Cavity Lining

The absorbed dose to the peritoneum is primarily a result of the emissions that are usually considered to be "nonpenetrating": beta particles (negative or positive), internal conversion electrons, and Auger electrons. The usual approach to

TABLE 5
Photon S-Values for Iodine-131 in Peritoneal Cavity Volume

Target organ	S-Value (mGy-MBq-sec)	S-Value (rad/μCi-hr)
Red marrow	5.2×10^{-7}	7.0×10^{-6}
Bone surfaces	3.0×10^{-7}	4.0×10^{-6}
Adrenals	1.5×10^{-6}	2.0×10^{-5}
Brain	1.4×10^{-9}	1.8×10^{-8}
Breasts	1.1×10^{-7}	1.5×10^{-6}
Lower large intestine wall	4.5×10^{-7}	6.0×10^{-6}
Small intestine	1.8×10^{-6}	2.4×10^{-5}
Stomach	1.1×10^{-6}	1.5×10^{-5}
Upper large intestine wall	1.6×10^{-6}	2.1×10^{-5}
Heart wall	7.0×10^{-7}	9.3×10^{-6}
Kidneys	1.2×10^{-6}	1.6×10^{-5}
Liver	9.9×10^{-7}	1.3×10^{-5}
Lungs	3.0×10^{-7}	4.1×10^{-6}
Ovaries	1.2×10^{-6}	1.7×10^{-5}
Pancreas	4.4×10^{-6}	5.8×10^{-5}
Remaining tissue (muscle)	4.1×10^{-7}	5.5×10^{-6}
Skeleton	2.3×10^{-7}	3.0×10^{-6}
Skin	9.8×10^{-8}	1.3×10^{-6}
Spleen	6.5×10^{-7}	8.7×10^{-6}
Testes	7.1×10^{-8}	9.4×10^{-7}
Thymus	1.2×10^{-7}	1.5×10^{-6}
Thyroid	1.7×10^{-8}	2.3×10^{-7}
Urinary bladder wall	7.7×10^{-7}	1.0×10^{-5}
Uterus	5.1×10^{-6}	6.8×10^{-5}
Total body	4.3×10^{-7}	5.7×10^{-6}

TABLE 6
Photon S-Values for Au-198 in Peritoneal Cavity Volume

Target organ	S-Value (mGy/MBq-sec)	S-Value (rad/μCi-hr)
Red marrow	5.5×10^{-7}	7.4×10^{-6}
Bone surfaces	3.1×10^{-7}	4.1×10^{-6}
Adrenals	1.6×10^{-6}	2.1×10^{-5}
Brain	1.3×10^{-9}	1.7×10^{-8}
Breasts	1.2×10^{-7}	1.6×10^{-6}
Lower large intestine wall	4.7×10^{-7}	6.3×10^{-6}
Small intestine	1.9×10^{-6}	2.6×10^{-5}
Stomach	1.2×10^{-6}	1.6×10^{-5}
Upper large intestine wall	1.7×10^{-6}	2.2×10^{-5}
Heart wall	7.4×10^{-7}	9.8×10^{-6}
Kidneys	1.3×10^{-6}	1.7×10^{-5}
Liver	1.0×10^{-6}	1.4×10^{-5}
Lungs	3.3×10^{-7}	4.3×10^{-6}
Ovaries	1.3×10^{-6}	1.8×10^{-5}
Pancreas	4.6×10^{-6}	6.2×10^{-5}
Remaining tissue (muscle)	4.3×10^{-7}	5.8×10^{-6}
Skeleton	2.3×10^{-7}	3.1×10^{-6}
Skin	1.1×10^{-7}	1.4×10^{-6}
Spleen	6.9×10^{-7}	9.2×10^{-6}
Testes	7.4×10^{-8}	9.9×10^{-7}
Thymus	1.2×10^{-7}	1.6×10^{-6}
Thyroid	2.1×10^{-8}	2.8×10^{-7}
Urinary bladder wall	8.3×10^{-7}	1.1×10^{-5}
Uterus	5.5×10^{-6}	7.3×10^{-5}
Total body	4.5×10^{-7}	6.0×10^{-6}

dose estimation for the surface of an organ or region which is assumed to contain a volume source of radioactive material is to estimate the surface dose as one half of the dose to the volume (*19*), which is good for most convex geometries. Another approach is to estimate the dose in the lining at various distances from the surface by consideration of point kernels (*20*). An average dose to the peritoneum for these radiations is not useful for evaluating dose effects, and a point kernel approach will be needed.

Loevinger et al. (*21*) gave models which can be used for calculating the dose from "infinite" plane sources at different perpendicular distances from the source. Because the extent of the source is large compared to the range of the electrons, this is an acceptable model of the lining of a large cavity. Berger (*20,22*) extended this work and presented information about the attenuation of electrons and betas in tissue. Cross et al. (*23*) have calculated the dose rate in water for many different beta-emitting radionuclides; however, they did not present information about radionuclides such as ^{99m}Tc that do not emit betas. We have developed a computer program based on Berger's work in MIRD Pamphlet No. 7 (*22*) that allows us to calculate the dose in tissue at various depths beyond the surface of the cavity if we assume that the source is uniformly distributed over the surface in a layer so thin that the source material itself does not attenuate the radiations. This distribution might be encountered if activity is administered in a small volume into a normal cavity. We further assume that the plane source is of infinite width relative to the range of the electrons or betas emitted.

The basic equation used is (*20*):

$$D(x) = 2 \pi \sigma \int_x^{R_m} y\, J(Y)\, dy,$$

where

- $D(x)$ = absorbed dose or dose rate at distance x for a thin plane source as described above;
- R_m = the maximum particle range;
- σ = the activity concentration per unit area;
- $J(y)$ = the point source dose function;
- $J(y) = n\, k\, E\, \Phi = n\, k\, E \dfrac{F(x,x_{90})}{4 \pi \rho\ x^2\ x_{90}}$
- n = the abundance of emissions with energy E;
- k = the proportionality constant to convert energy per gram to the desired absorbed dose units;
- $F(x,x_{90})$ = Berger's point source scaled absorbed dose distribution [from (*22*)];
- x_{90} = the 90th percentile distance for emissions with energy E, i.e., the distance within which 90% of the emitted energy is absorbed, and
- ρ = the medium density.

Several researchers have shown that the radioactivity may *not* be uniformly distributed in all cases (*6,9,16,24*). The estimates presented in this report will be valid for the areas where the activity is uniformly distributed at a given area concentration; other areas may receive little or no absorbed dose.

Another problem associated with calculating the dose to the cavity lining from activity on the surface is making a reliable estimate of the surface area of the lining. Estimates have ranged from ~5,000 cm^2 to 30,000 cm^2 (*25*). The radiation dose along a line perpendicular to a plane source is directly proportional to the activity area concentration (e.g., Bq/cm^2). If the activity is assumed to be distributed in a uniformly thin layer on the surface, the doses would be inversely proportional to the surface area; that is, the doses for a 5,000 cm^2 surface area would be six times greater than the doses for a 30,000 cm^2 surface area. Our results are expressed as absorbed dose rate per unit area concentration to facilitate scaling based on the surface area assumed to be involved. These results will be valid only for areas where the model assumptions are met; because of the considerable folding of the peritoneum, overlap of source regions may result in dose distributions not predicted by this model. Also, the assumption that the doses shown may be directly related to surface area is limited strictly to lines running perpendicular to the surface near the center of a large surface distributed source. Some loss of accuracy is necessarily anticipated near the edges of distributed sources.

For the situations in which the cavity contains large amounts of fluid, Loevinger et al. (*21*) presents a model for a semi-infinite plane source of finite thickness which may be applied to this situation. In this case, the radionuclide *volume* concentration will be the critical quantity, and some of the energy from nonpenetrating emissions will be attenuated in the source itself. In this case, the basic equation is (*21*):

$$D_t(x) = \int_x^{x+h} \frac{\rho\, \tau\, D(y)}{\sigma}\, dy$$

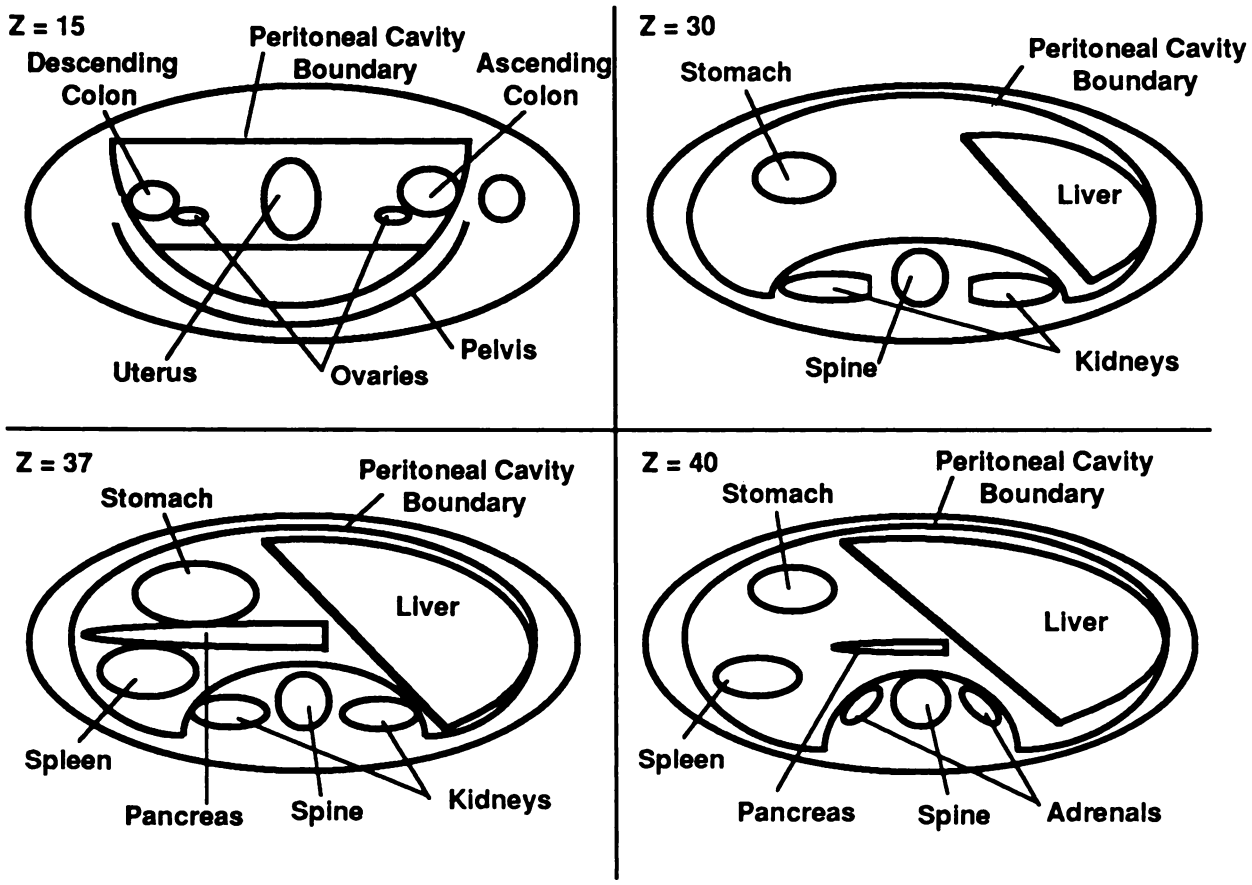

FIGURE 1
Computer generated drawings of cross sections of the Fisher-Snyder phantom at Z = 15, 30, 37, and 40 cm, showing the placement of the peritoneal cavity model.

where

$D_t(x)$ = the dose from a thick plane source;
h = the thickness of the plane source;
τ = the activity per unit volume;
D(y) = the expression shown above for the thin plane source; and
σ = the activity per unit area, from the expression above.

RESULTS

Specific absorbed fractions derived from the Monte Carlo calculations are presented in Table 1. Values are given for the discrete energies listed in the previous section; interpolation between the values is necessary for use with actual gamma ray and x-ray energies.

TABLE 7
Electron Doses in the Peritoneal Cavity Wall from Surface and Volume Distributed Sources of ^{32}P

Distance (cm)*	Surface source		Volume source	
	(mGy-cm^2/MBq-sec)	(rad-cm^2/μCi-hr)	(mGy-g/MBq-sec)	(rad-g/μCi-hr)
0.0	—	—	0.056	0.74
0.006	0.75	10	0.050	0.66
0.018	0.53	7.0	0.042	0.56
0.030	0.42	5.6	0.037	0.49
0.12	0.15	2.0	0.014	0.19
0.21	0.064	0.85	0.0050	0.067
0.30	0.023	0.31	0.0014	0.018
0.40	0.0047	0.062	0.00013	0.0017

* Distance from peritoneal cavity into cavity wall.

TABLE 8
Electron Doses in the Peritoneal Cavity Wall from Surface and Volume Distributed Sources of ^{90}Y

Distance (cm)*	Surface source		Volume source	
	(mGy-cm²/MBq-sec)	(rad-cm²/μCi-hr)	(mGy-g/MBq-sec)	(rad-g/μCi-hr)
0.0	—	—	0.075	1.0
0.006	0.83	11	0.069	0.92
0.018	0.56	7.4	0.062	0.82
0.030	0.45	6.0	0.056	0.74
0.12	0.20	2.7	0.029	0.39
0.21	0.11	1.5	0.015	0.20
0.30	0.065	0.86	0.0075	0.10
0.40	0.032	0.42	0.0030	0.040

* Distance from peritoneal cavity into cavity wall.

S-values for photon emissions from ^{99m}Tc, ^{111}In, ^{125}I, ^{131}I, and ^{198}Au are presented in Tables 2 through 6. Electron doses to the cavity wall in absorbed dose per disintegration are listed for ^{32}P, ^{90}Y, ^{99m}Tc, ^{111}In, ^{125}I, ^{131}I, and ^{198}Au in Tables 7 through 13 for both plane and volume distributed sources. For the volume distributed sources, the predicted surface dose (one half of the dose to the volume) is also given. The values are expressed as absorbed dose rate (mGy/sec) per unit area or volume concentration (MBq/cm² or MBq/g), resulting in units of mGy-cm²/MBq-sec or mGy-g/MBq-sec.

DISCUSSION

The photon specific absorbed fractions are of the same order of magnitude as values for the whole body for moderate energies, but do show significant variation among organs near the abdominal cavity and those farther away. As is usual, values at low energy become vanishingly small for organs far from the cavity (values less than 10^{-13} g^{-1} were set equal to zero in Table 1). In general, the adrenals, pancreas, uterus, ovaries, and gastrointestinal organs tend to have the highest specific absorbed fractions. Although the adrenals are considered to be outside of the cavity, they are adjacent to the invaginations of the cavity near the spine (Fig. 1). The fact that the uterus and ovaries also absorb considerable fractions of the energy emitted from the cavity is significant in situations involving women of childbearing years [although the peritoneal cavity will not be a major contributor of absorbed dose to these organs in hysterosalpingography studies (26)].

The absorbed dose rate functions for nonpenetrating emissions are sensitive to the range of the radiations (Tables 7 through 13). Emissions of ^{125}I are rapidly absorbed in the first few micrometers of tissue, while the emissions of ^{32}P and ^{90}Y may penetrate to several millimeters, which may be beyond the bounds of the cavity wall. This raises the possibility that some organs outside of the cavity may receive a dose from the "nonpenetrating" emissions originating within the cavity. The variability in the activity distribution in different studies and patients makes it difficult to identify which organs may be irradiated in this way and what the absorbed doses might be. It is clear that only a small portion of the organ's exterior will receive a dose because the values are falling off rapidly at these distances from the cavity. Because of spatial variation, the biologic significance of these values is difficult to evaluate given the current understanding of radiation dose and

TABLE 9
Electron Doses in the Peritoneal Cavity Wall from Surface and Volume Distributed Sources of ^{99m}Tc

Distance (cm)*	Surface source		Volume source	
	(mGy-cm²/MBq-sec)	(rad-cm²/μCi-hr)	(mGy-g/MBq-sec)	(rad-g/μCi-hr)
0.0	—	—	0.0013	0.017
0.001	0.15	2.0	0.00090	0.012
0.002	0.12	1.6	0.00075	0.010
0.004	0.096	1.3	0.00056	0.0075
0.008	0.062	0.82	0.00025	0.0033
0.012	0.029	0.38	0.000067	0.00089
0.016	0.0044	0.059	0.0000074	0.000099
0.020	0.00034	0.0045	0.00000041	0.0000055

* Distance from peritoneal cavity into cavity wall.

TABLE 10
Electron Doses in the Peritoneal Cavity Wall from Surface and Volume Distributed Sources of ^{111}In

Distance (cm)*	Surface source		Volume source	
	(mGy-cm²/MBq-sec)	(rad-cm²/μCi-hr)	(mGy-g/MBq-sec)	(rad-g/μCi-hr)
0.0	—	—	0.0028	0.037
0.002	0.22	2.9	0.0019	0.025
0.004	0.16	2.1	0.0016	0.021
0.007	0.11	1.5	0.0012	0.016
0.018	0.034	0.45	0.00036	0.0048
0.040	0.0024	0.032	0.000098	0.00013
0.050	0.00011	0.0015	0.00000029	0.0000039

* Distance from peritoneal cavity into cavity wall.

TABLE 11
Electron Doses in the Peritoneal Cavity Wall from Surface and Volume Distributed Sources of ^{125}I

Distance (cm)*	Surface source		Volume source	
	(mGy-cm²/MBq-sec)	(rad-cm²/μCi-hr)	(mGy-g/MBq-sec)	(rad-g/μCi-hr)
0.0	—	—	0.0016	0.021
0.0001	2.2	29	0.00083	0.011
0.0005	0.74	9.9	0.00036	0.0048
0.001	0.17	2.3	0.000096	0.0013
0.002	0.0024	0.032	0.00000032	0.0000043

* Distance from peritoneal cavity into cavity wall.

TABLE 12
Electron Doses in the Peritoneal Cavity Wall from Surface and Volume Distributed Sources of ^{131}I

Distance (cm)*	Surface source		Volume source	
	(mGy-cm²/MBq-sec)	(rad-cm²/μCi-hr)	(mGy-g/MBq-sec)	(rad-g/μCi-hr)
0.0	—	—	0.015	0.20
0.001	1.3	17	0.014	0.18
0.003	0.75	10	0.011	0.15
0.006	0.53	7.0	0.0090	0.12
0.018	0.24	3.2	0.0050	0.066
0.030	0.14	1.8	0.0028	0.037
0.050	0.057	0.76	0.00105	0.014
0.080	0.012	0.16	0.00015	0.0020

* Distance from peritoneal cavity into cavity wall.

TABLE 13
Electron Doses in the Peritoneal Cavity Wall from Surface and Volume Distributed Sources of ^{198}Au

Distance (cm)*	Surface source		Volume source	
	(mGy-cm²/MBq-sec)	(rad-cm²/μCi-hr)	(mGy-g/MBq-sec)	(rad-g/μCi-hr)
0.0	—	—	0.026	0.35
0.001	1.2	16	0.024	0.32
0.003	0.83	11	0.022	0.29
0.006	0.65	8.6	0.020	0.26
0.018	0.37	4.9	0.014	0.18
0.030	0.26	3.4	0.010	0.14
0.080	0.075	1.0	0.0030	0.040
0.12	0.030	0.40	0.00098	0.013

* Distance from peritoneal cavity into cavity.

effects. Approximate thresholds for nonstochastic effects in several whole organs are fairly well known (27); models for stochastic effects, while involving considerable uncertainties, may be represented mathematically for average organ or whole-body doses (*28*). No definitive work has been done, however, which relates risk to spatially distributed absorbed doses.

When the dose conversion factors for the particulate radiations (mGy-cm^2/MBq-sec or mGy-g/MBq-sec) are expressed as absorbed dose per unit cumulated activity (mGy/MBq-sec) by dividing by 5000 cm^2 or 4000 g, they tend to be a few orders of magnitude higher than the photon S-values, especially at short distances. Therefore, the principal dose to the cavity wall is from the beta and electron components.

SUMMARY

We have developed a mathematical model of the peritoneum and the peritoneal cavity to be used for calculating radiation dose to the major organs in the abdomen. This model should provide useful dosimetric information in situations in which a significant amount of activity may enter the peritoneal cavity. The absorbed dose to the cavity wall is mostly defined by the nonpenetrating emissions. These values are sensitive to the range of the emissions from a particular radionuclide. The photon absorbed doses to major organs of the body are of the same order of magnitude as those from activity in the total body, but the variations are significant. The adrenals, pancreas, ovaries, uterus, and gastrointestinal organs receive higher absorbed doses per disintegration than other organs and organ systems.

ACKNOWLEDGMENT

This work was performed for the U.S. DOE under contract DE-AC05-76OR00033 and Interagency Agreement No. FDA 224-75-3016, DOE 40-286-71.

REFERENCES

1. Root SW, M Tyor, G Andrews, et al. Distribution of colloidal radioactive chromic phosphate after intracavitary administration. *Radiology* 1954; 63:251–259.
2. Lange RH, J Shields, H Rozendahal. Colloidal radioactive chromic phosphate in the control of malignant effusions. *NY State J Med* 1956; 56:1928–1931.
3. O'Bryan RM, R Talley, M Brennan, et al. Critical analysis of the control of malignant effusions with radioisotopes. *Henry Ford Hosp Med* 1968; 16:3.
4. Singh A, Grossman Z, McAfee J, Thomas D. LeVeen shunt patency studies: clarification of scintigraphic findings. *Clin Nucl Med* 1980; 5:106–108.
5. Baum S, Avignon M. Radionuclides and LeVeen shunt patency. *Clin Nucl Med* 1979; 4:486.
6. Farrer P, Friede J, Wexler M. Scintiphotographic evaluation of LeVeen peritoneo-venous shunt patency using intraperitoneal Tc-99m-MAA. *Clin Nucl Med* 1979; 4:451–454.
7. Crawford K, McDougall I. Prediction of satisfactory response to pleural sclerosis using radiopharmaceuticals—study in a patient with cirrhotic hydrothorax and LeVeen shunt. *Arch Intern Med* 1982; 142:194–196.
8. Abdel-Dayhem H. False ascites in a patient with LeVeen shunt detected by intraperitoneal injection of Tc-99m-sulfur colloid. *Clin Nucl Med* 1979; 4:1–2.
9. Bolitho L, Andrews J, Lichtenstein M. The intraperitoneal use of technetium sulfur colloid. *Aust Radiol* 1981; 25:159–161.
10. Madeddu G, Ovidio N, Casu R, et al. Evaluation of peritoneovenous shunt patency with Tc-99m labeled microspheres. *J Nucl Med* 1983; 24:302–307.
11. McCalley M, Braunstein P, Stone S, et al. Radionuclide hysterosalpingography for evaluation of fallo pian tube patency. *J Nucl Med* 1985; 26:868–874.
12. Snyder WS, Ford M, Warner G, Fisher, Jr, H. Estimates of absorbed fractions for monoenergetic photon sources uniformly distributed in various organs of a heterogeneous phantom. MIRD Pamphlet No. 5. *J Nucl Med* (suppl 3):1969.
13. Cristy M, Eckerman K. Specific absorbed fractions of energy at various ages from internal photon sources. ORNL/TM-8381, Oak Ridge National Laboratory, Oak Ridge, TN, 1987.
14. Anson B, ed. *Morris' human anatomy.* New York: McGraw-Hill Book Company, 1966.
15. Stark P. *Introduction to numerical techniques.* New York: Macmillan, 1970.
16. Walton R, Sinclair W. Intracavitary irradiation with radioactive colloidal gold in the palliative treatment of malignant pleural and peritoneal effusions. *Br Med Bull* 1952; 8:165–171.
17. Williams L, Wong J, Findley D, Forell B. Brake radiation dose due to Y-90 measured in an anthromorphic phantom [Abstract]. *J Nucl Med* 1987; 28:684.
18. Stabin M, Eckerman K, Ryman J, Williams L. Bremsstrahlung dosimetry component in Y-90 monoclonal antibody therapy [Abstract]. *J Nucl Med* 1988; 29:859.
19. Synder WS, Ford M, Warner G, Watson S. "S," absorbed dose per unit cumulated activity for selected radionuclides and organs. *MIRD Pamphlet No. 11.* Society of Nuclear Medicine, 1975.
20. Berger M. Beta-ray dosimetry calculations with the use of point kernels. In: Cloutier R, Edwards C, Snyder W, eds. In *Medical radionuclides: radiation dose and effects.* CONF-691212, U.S. Atomic Energy Commission Division of Technical Information, 1970.
21. Loevinger R, Japha E, Brownell G. Discrete radioisotope sources. In: Hine G, Brownell G, eds. In: *Radiation dosimetry.* Chap. 16. New York: Academic Press, 1958:694–753.
22. Berger M. Distribution of absorbed dose around point sources of electrons and beta particles in water and other media. *MIRD Pamphlet No. 7. J Nucl Med* (suppl 5):1971.
23. Cross W, Ing H, Freedman N, Mainville J. Tables of beta-ray dose distributions in water, air, and other media. Ontario, Atomic Energy of Canada Limited AECL-7617, 1982.
24. Andrews G, Root S, Kniseley R. Metabolism and distribution of colloidal Au-198 injected into serous

cavities for treatment of effusions associated with malignant neoplasms. *Cancer* 1953; 6:294–302.
25. Rosenshein N, Blake D, McIntyre P, et al. The effect of volume on the distribution of substances instilled into the peritoneal cavity. *Gynecol Oncol* 1978; 6:106–110.
26. Stabin M. Radiation dosimetry in radionuclide hysterosalpingography with Tc-99m. *J Nucl Med* 1989; 30:415–416.
27. United Nations Scientific Committee on the Effects of Atomic Radiation: Sources and Effects of Ionizing Radiation. United Nations, New York, 1982.
28. International Commission on Radiological Protection: Recommendations of the International Commission on Radiological Protection, ICRP Publication 26. Pergamon Press, New York, 1977.